Influence of suprathermal background electrons on strong auroral double layers: Observations

L. Andersson,[1] D. L. Newman,[2] R. E. Ergun,[1,3] M. V. Goldman,[2]
C. W. Carlson,[4] and J. P. McFadden[4]
[1]*Laboratory for Atmospheric and Space Physics, University of Colorado, Boulder, Colorado 80309, USA*
[2]*Center for Integrated Plasma Studies, University of Colorado, Boulder, Colorado 80309, USA*
[3]*Department of Astrophysical and Planetary Sciences, University of Colorado, Boulder, Colorado, USA*
[4]*Space Science Laboratory, University of California, Berkeley, California 94729, USA*

(Received 15 October 2007; accepted 1 May 2008; published online 1 July 2008)

This study examines the properties and evolution of strong, laminar double layers in the downward current region of the aurora and present several previously unpublished events from the Fast Auroral SnapshoT (FAST) satellite. Analysis of an event is presented for which the FAST satellite appears to have dwelled on the high-potential side (high-altitude side) of a double layer for an extended period, suggesting that a small (few percent of density) background of suprathermal electrons can strongly influence the structure and stability of double layers. From these observations, it is inferred that the accelerated electrons can be accelerated by either of two classes of double layers: (1) self-regulated double layers (varying field-aligned potential, with weak or no suprathermal electron background) or (2) externally regulated double layers (less variable field-aligned potential, with significant suprathermal electron background). Elements of the interpretation presented here are supported by numerical simulations, as reported in two accompanying papers. © *2008 American Institute of Physics*. [DOI: 10.1063/1.2938751]

I. INTRODUCTION

Parallel electric fields have been a research topic for decades and the focus of many studies of auroral acceleration. One configuration of a localized parallel electric field in a current-driven plasma is known as a double layer (DL). The name comes from the separation of charges in a narrow layer that gives rise to a localized unipolar parallel electric field. A commonly used solution for an ideal static DL, called a Bernstein–Greene–Kruskal[3] (BGK) solution, can be derived using four (or more) particle populations from the time-independent Vlasov–Poisson equations. This type of configuration is the subject of a review by Raadu.[4] In early studies associated with auroral acceleration, U-shaped potential structures were suggested and motion of the DL was theorized.

A subgroup of DLs, designated strong DLs, are of special interest since they can accelerate particles over short distances to energies well above their initial thermal energies. In space plasmas, in contrast to laboratory plasmas and theoretical studies, strong DLs have eluded conclusive observations until recently.[5–7] Observations in space of weak DLs, or asymmetric solitary waves, were reported several decades ago[8,9] but could not account for the observed level of particle acceleration in the auroral region.[10] It has also been shown that large asymmetric solitary waves do not have a net potential[11] suggesting that previously reported weak DLs may not be DLs at all. In this paper, we examine observations of strong double layers in the downward current region of the aurora. We present evidence that a small to moderate suprathermal population of electrons can greatly influence their behavior.

A. Model of the downward current region of the aurora

A schematic depicting the regions associated with a strong DL is presented in Fig. 1. The schematic is based on earlier observational and numerical studies of DLs from the downward current region of the aurora.[5,6,12] In the cartoon, the DL is at the bottom of a large-scale U-shaped potential structure. The parallel electrostatic potential is in the region indicated as the "ramp" with a thickness of $O(10)$ Debye lengths. This potential ramp is well separated from the turbulent region if the DL is laminar. The electric field ($\boldsymbol{E}$) associated with this potential is in the direction normal to the thin ramp layer. At high altitudes, $\boldsymbol{E}$ is primarily perpendicular to the magnetic field ($\boldsymbol{B}$) but has a substantial parallel component at the bottom of the potential structure. The parallel electric field causes the ions to be accelerated Earthward and electrons to be accelerated anti-Earthward (downward and upward in the illustration). How the different particle populations are moving with respect to the ramp region was illustrated in Fig. 7 in Ref. 6 and is described in words below.

Space measurements have shown that the observed DLs are often oblique[5,6,8,13,14] supporting the U-shaped description illustrated in Fig. 1. The obliqueness of the DL does not affect the behavior of the strongly magnetized electrons. However, the weakly magnetized ions may experience perpendicular heating as they pass through the oblique ramp region.

The accelerated electrons form a beam that penetrates the hot magnetospheric plasma on the high-potential side of the DL. The emerging electron beam will drive convective wave growth. The nature of these instabilities and how fast

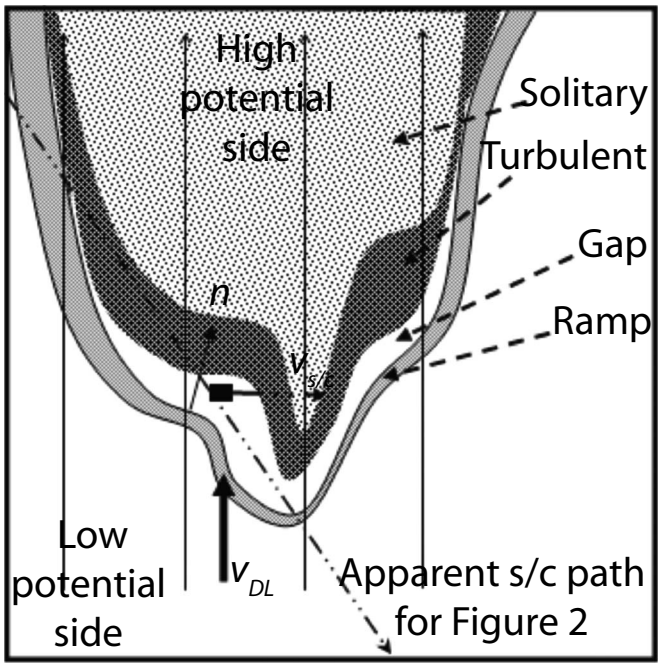

FIG. 1. A complex U-shaped potential structure is depicted schematically with associated regions labeled accordingly. In the illustration the apparent spacecraft path drawn is characteristic of that inferred for each of the potential crossings presented in Fig. 2. The apparent path is the result of the dominantly horizontal satellite motion combined with an anti-Earthward motion of the potential structure.

they will grow depends on the relationship between the electron beam and the suprathermal background electron population.[15,16] In the region adjacent to the high-potential side of the DL, observations suggest that the convectively unstable waves have not yet attained significant amplitude. This region is designated the "gap region" in Fig. 1 because of the lack of observed electric field fluctuations or waves. The size (thickness) of gap region is roughly $O(10-100)$ Debye lengths. Within this gap region, the electron distribution can have an unstable positive slope.

The waves driven by convective instabilities will grow linearly until they reach sufficient amplitude for wave-particle interactions to dominate. The region in which these strong wave-particle interactions are occurring is designated the "turbulent region" in Fig. 1. In the turbulent region, the electron distribution loses its free energy and a positive slope is no longer observed. The thermalization of the beam has also been verified in Vlasov simulations of the upward current region.[17]

A fraction of the initial electron beam is redirected back from the turbulent region toward the DL. This Earthward-drifting population together with slower electrons originating on the high-potential side of the DL is reflected back anti-Earthward by the DL's electric field. (These electrons with energies less than the DL potential are denoted as the "trapped" population in the BGK solution[3]). The relaxation of the electron beam distribution and consequent saturation of the waves occurs via trapping rather than from quasi-linear plateau formation.[12] The saturated electron distribution is characterized by vortexlike regions of trapped electrons referred to as electron phase-space holes (or more compactly as simply electron holes). These electron holes are initially closely packed and can interact with one another via "merging" events. Sufficiently far from the ramp, only isolated holes remain. These well-defined electron holes are commonly observed in what is designated the "solitary wave region" in Fig. 1, where they move away from the ramp and gap regions with a velocity of order of the electron beam velocity.[18]

B. Static parallel electric fields

A satellite that crosses far from the bottom of the U-shaped potential illustrated in Fig. 1, the most common case, would encounter diverging perpendicular electric fields with anti-Earthward accelerated field-aligned electrons populating the region between the diverging electric fields.[19] If the potential structure is static, the measured perpendicular electric field provides information about the parallel potential drop ($\Delta\Phi_{\|}$) at the bottom of the potential structure. In such a case, the energy that the electrons have gained passing through the parallel electric field will be $e\Delta\Phi_{\|}$, directly proportional to the potential across the integrated perpendicular electric field.

This proportionality has been verified by some event studies[18,20] and a larger statistical study.[21] These studies indicate that approximately half of the regions where anti-Earthward accelerated electrons are observed can be regarded as static. For the remaining events, the U-shaped potential structures are either evolving on time scales comparable to the observation time, or the downward currents are changing. Theses studies have shown that one can use the characteristic energy of the electrons to infer a potential across an assumed DL if one avoids events where there are clear signs of activity such as Alfvén waves.

A laminar DL is not the only plasma structure that maintains a parallel electric field. By laminar DL we mean a "monotonic" potential across the ramp as illustrated in Fig. 1. When a potential across the ramp region is not monotonic we refer to it as a turbulent DL (despite the fact that the charge density has a more complex structure than an ideal DL). In a current-driven open boundary simulation, turbulent DLs have been observed prior to the development of a laminar DL.[12] Alternatively, turbulent DLs may result from the disruption of a laminar state.[1] The turbulent DL typically lacks a well-formed gap region such as is illustrated in Fig. 1. Thus, if a satellite does not encounter the parallel electric field itself, the presence of the gap region is one of the best ways to distinguish between electron acceleration by a laminar DL and a turbulent DL. A positive slope in the electron distribution in a gap region is favorable evidence of a laminar DL.

C. Organization

We start the remainder of the paper with a review of observations in the context of DL theory and then present four additional previously unpublished observations of localized parallel electric fields in order to supplement those in the published literature.[5,6] In Sec. III, a long-duration observation from the high-potential side of a potential structure is

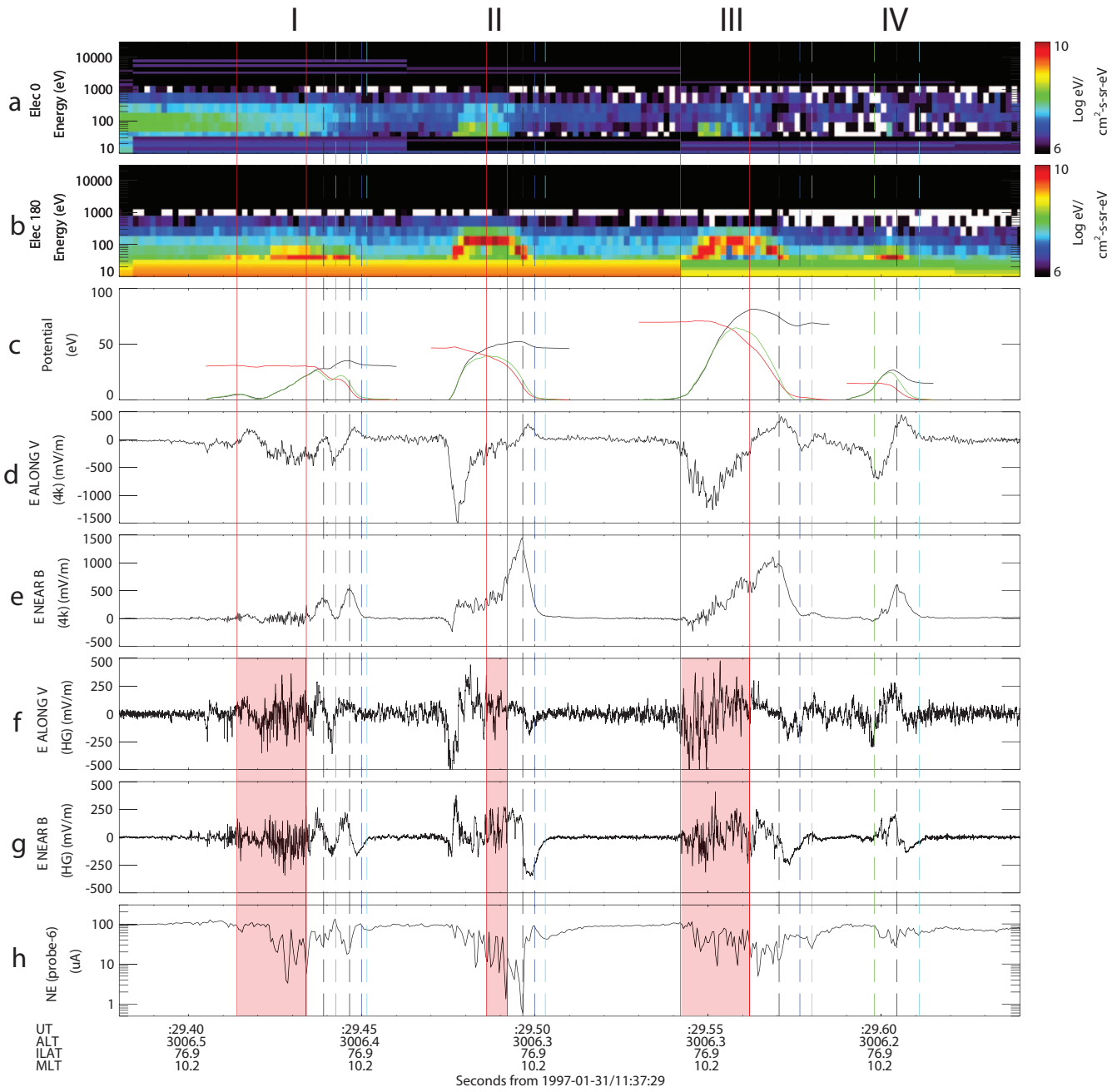

FIG. 2. (Color) One observation during which FAST traverses four potential structures. Each potential structure is associated with a localized parallel electric field. The panels present the field aligned electron spectra [Earthward in panel (a) and anti-Earthward in panel (b)]. Panel (c) is the derived potential from the DC electric field measurement. Panels (d) to (g) are the DC and AC electric field measurements for the parallel and the perpendicular directions. Panel (h) presents the Langmuir probe current which to the first order can be interpreted as representing the electron density. See text for further details.

discussed. We identify three distinct time periods within this observation, each characterized by a different suprathermal background electron population. The following sections contain analyses of particle and wave measurements during these three time periods. Section IV A describes a period when no significant suprathermal background is observed, whereas Secs. IV B and IV C describe periods when there is significant suprathermal background, but of differing character. The correlation between the inferred DL potential and properties of the suprathermal background electron population is considered in Sec. V. Finally, the key implications of suprathermal background electrons on DLs in the downward current region are summarized in Sec. IV. The observations presented in this paper are made by the FAST satellite.[22] Detailed information about the FAST instruments can be found in Carlson *et al.*,[23] Ergun *et al.*,[24] and Elphic *et al.*[25]

II. DIRECT OBSERVATIONS DOUBLE LAYERS

There have been but a few reported in situ observations of strong parallel electric fields from the downward current region (e.g., Refs. 5 and 6). Here, we supplement these with additional observations of direct observations of parallel

electric fields shown in Fig. 2. The horizontal axis in Fig. 2 represents 0.260 s of time, during which, only ~3 particle spectra (48 energies with 72 ms time resolution) are recorded by the electron (EESA) and ion electrostatic analyzer[23] on the FAST spacecraft. However, coarse six-energy electron pitch angle distributions with 1.6 ms time resolution are available from the stepped electrostatic analyzer (SESA) instrument.[23]

Panels 2(a) and 2(b) present merged data from the EESA and SESA instruments. The SESA covers the energy range between 34 eV and 1.3 keV and EESA data are presented outside this range; the three lowest energy levels of the SESA are: 34–41, 67–82, and 133–165 eV. Figure 2(a) displays Earthward (nearly field-aligned) energy spectrum $(0° \pm 22°)$ and Fig. 2(b) the anti-Earthward energy spectrum $(180° \pm 22°)$. When merging the EESA and the SESA data in Panels 2(a) and 2(b), a small correction has been introduced to the SESA measurements to match the EESA fluxes.

Figure 2(c) plots the electric potential derived from the integrated electric field signals. The potential derivation is described in detail below. Figures 2(d) and 2(e) plot the DC <4 kHz bandpass filtered (d) perpendicular and (e) near-parallel electric field. Figures 2(f) and 2(g) plot the same signals with >100 Hz and <16 kHz bandpass filtering. The near-parallel electric field signals in Fig. 2(e) indicate geophysical parallel electric fields.[5] Figure 2(h) shows the current from one of the Langmuir probes, which can be used as an indication of the plasma density.

The data in Fig. 2 are interpreted as consisting of four separated potential structures that are passing the satellite with motion along $\boldsymbol{B}$ as the satellite moves primarily perpendicular to $\boldsymbol{B}$. The four potential structures are labeled I–IV in the observed order (see top of Fig. 2). They are most easily identified by the four time periods when the parallel electric field is nonzero [panel 2(e)]. The peaks of the parallel electric fields are marked by black, dashed vertical lines; there are two peaks in event I. The peaks in the parallel electric field are in regions of density depletions.

The electrostatic potential [Fig. 2(c)] is calculated from both the parallel and perpendicular electric fields and the relative motion of the structure:

$$\Delta\Phi = \int_{t_0}^{t} \vec{E} \cdot \vec{v} dt = \int_{t_0}^{t} E_{\perp} v_{\perp} dt + \int_{t_0}^{t} E_{\parallel} v_{\parallel} dt. \quad (1)$$

The calculation is broken into two parts. If we assume that the structures are not moving perpendicular to $\boldsymbol{B}$ (see, for example, Ref. 5), part of the potential can be derived from $E_{\perp}$ and the spacecraft velocity $v_{\perp} \cong v_s$, which is primarily perpendicular to $\boldsymbol{B}$. This contribution to the right side of Eq. (1) is plotted as a black line in Fig. 2(c). The relative velocity $v_{\parallel}$ of the structure parallel to $\boldsymbol{B}$ can be estimated by adjusting its value until $\Delta\Phi$ from Eq. (1) vanishes on both sides of the structure. These velocities are determined for events I to IV to be anti-Earthward with magnitudes of 8.5, 3.7, 4.6, and 4.6 km/s, respectively, which are close to the nominal ion acoustic speed. The red lines plot the contribution from $E_{\parallel}$ and the green lines indicate the sum of the contribution to the total potential. The peak potentials have the values 22, 40, 65, and 25 V, respectively. These net potential values agree well with the peak energies in the SESA observations in Fig. 2(b), with the exception of event II where they differ by a factor of 2 (40 V potential with 80 eV electron energies).

The red shaded areas delineated by the vertical red lines mark periods when the electric field measurements may have experienced AC saturation. The signals reach the maximum of the A/D converter as a result of electron phase-space holes having extremely intense fields. However, saturation can influence the accuracy of the density measurements as well as the electric field measurements, in the red-shaded regions. Fortunately, the most intense turbulence associated with the largest electron holes is not co-located with the DC parallel electric fields. The conclusions of this article take the possibility of saturation into account.

All four of the events are consistent with the pattern depicted in the schematic of Fig. 1. The structures are moving anti-Earthward, so the apparent path of the spacecraft is downward in the frame of the potential structure. At the left boundaries, anti-Earthward electron beams are observed in conjunction with a negative $E_{\perp}$ (opposite to the spacecraft velocity). The spacecraft appears to have entered the sides of the structures, after which electron phase-space holes and intense turbulence are observed. As $E_{\parallel}$ peaks, electron phase-space holes are no longer seen and the turbulence level is weaker. In events II and III, positive slopes in the electron distribution (not shown) were observed just before $E_{\parallel}$ peaked. The peaks in $E_{\parallel}$ coincide with lower current to the Langmuir probes indicating density depletions. Local density minima (Fig. 2, light blue vertical lines) and local maxima (dark blue vertical lines) are both observed. Density fluctuations on the low potential side of the DL are discussed in the accompanying simulation paper.[2]

The events in Fig. 2 are similar to previously reported double layers in the downward current region of the aurora.[5,6,26] Event I, however, is somewhat different in that it has a double peak. The potential structure is nearly monotonic with a midplateau [red line in Fig. 2(c)]. This double peak feature is not currently understood.

III. PLASMA CONDITIONS DURING DOUBLE LAYER OBSERVATIONS

Here we examine the influence of the suprathermal electron population on DLs. For example, a suprathermal electron population is present at the beginning of the plot in Fig. 2 [near left edge of panel (a), between 30 and 300 eV]. The flux of this population fades by the end of this event (compare 29.39 UT with 29.65 UT). This reduction could be caused by a potential drop at higher altitudes. An analysis of the electron distribution (not shown) reveals that the suprathermal background electron population has a temperature of ~100 eV. At the beginning of Fig. 2, the ~100 eV suprath-

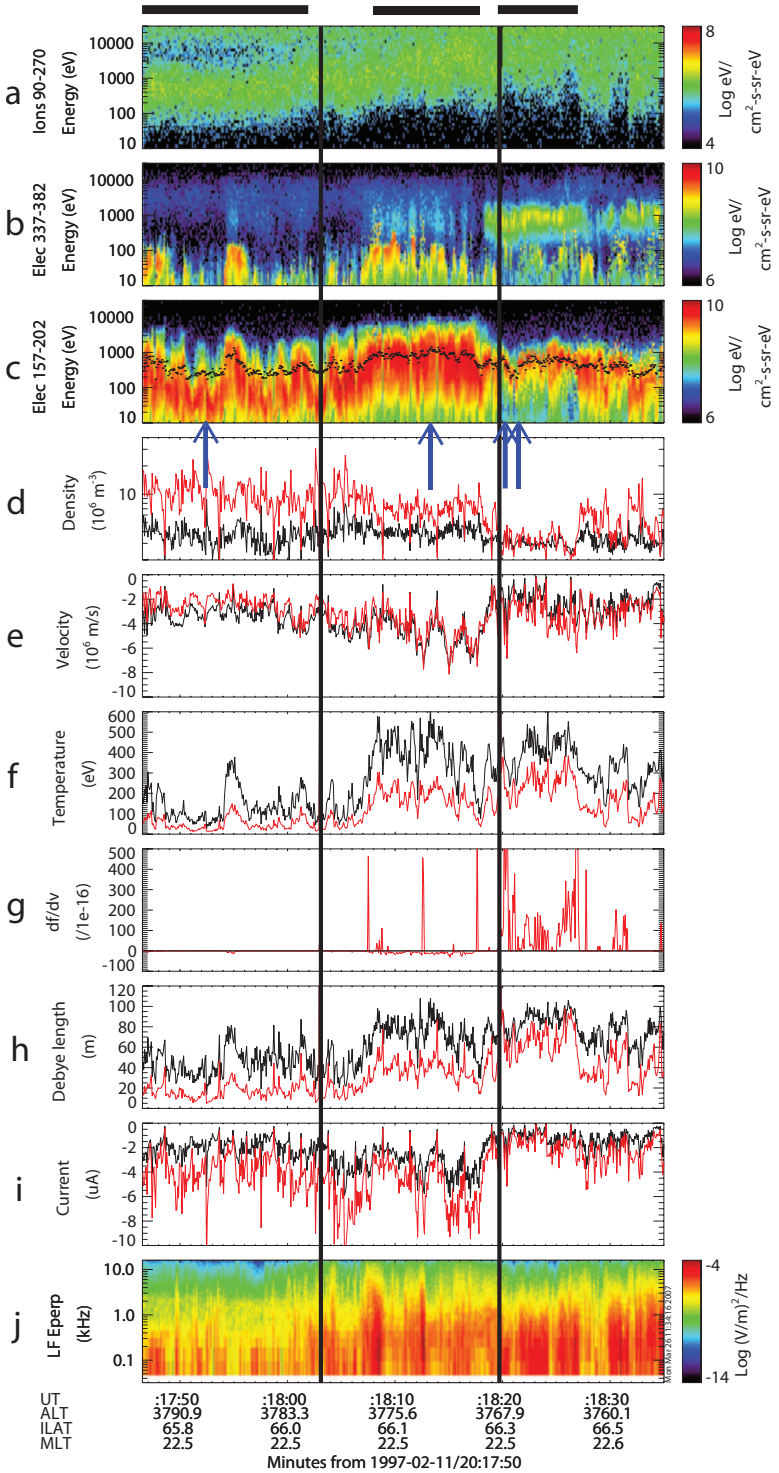

FIG. 3. (Color) An anti-Earthward enhanced field-aligned electron flux event is presented with the panels from top to bottom as follows: (a) the anti-Earthward ion energy-flux spectrum; (b) the Earthward electron energy-flux spectrum; (c) the anti-Earthward electron energy flux-spectrum; (d) to (f) the calculated moments of density, velocity, and temperature, respectively; (g) the largest positive slope in the one dimensional reduced parallel electron distribution; (h) the local Debye length; (i) the estimated current from the electron measurement; and (j) the perpendicular wave spectrum. The black lines in panels (d) to (i) are derived from the measured 2D distribution and the red line from the calculated 1D reduced distribution. The four arrows below panel (c) mark the times at which the four distributions presented in Fig. 4 are measured. The black vertical lines are time intervals with data gaps. See text for additional details.

ermal background population is clearly visible; it is isotropic with a empty loss cone. During events I and II, the suprathermal background population is reduced. Later on, the suprathermal background population disappears and only the upward mirrored part remains.

The simultaneous observation of double layers and enhancements in the suprathermal electron population as seen in Fig. 2 suggests a possible connection between these two phenomena. A single observation period ideally suited for delineating correlations between the characteristics of DLs and changes in the suprathermal background electron population and is explored in depth in the reminder of this section.

A. Downward current region observations with a varying suprathermal electron background

The event in Fig. 3 has been selected to illustrate the effect of external suprathermal background electrons on a DL in the downward current region. In this event, anti-

Earthward-flowing electrons are continuously observed for more than 50 s, corresponding to a perpendicular distance of ~300 km at the satellite altitude. The accelerated electrons indicate that the observation is made on the high-potential side of a DL.

The top panel of Fig. 3(a) displays the ion energy flux for anti-Earthward pitch angles $180° \pm 90°$. The field-aligned electron energy flux (from the EESA) for pitch angles within $0° \pm 22°$ (Earthward) and $180° \pm 22°$ (anti-Earthward) are plotted in panels (b) and (c), respectively. The calculated "characteristic" energy (W_c) of the electron distribution is indicated by black dots in panel (c). The characteristic energy is defined as $W_c = e\Psi/J$ and is derived from the anti-Earthward field-aligned energy flux (Ψ) and current density (J) based on the same pitch angle range that is plotted ($180° \pm 22°$). Other methods of calculating the characteristic energy have been employed elsewhere.[27] We evaluated these methods and found only minor differences in the statistical properties.

A small spin periodic (~5 s) modulation of the electron flux is detectable in Figs. 3(c), 3(d), and 3(i). This modulation is due to a combination of a narrow electron beam and a boom blocking the EESA detector (this only occur at limited spacecraft orientations) and is not geophysical in origin.

The calculated characteristic energy in Fig. 3(c) can serve as a proxy for the field-aligned potential Earthward of the satellite. The characteristic electron energy is constantly changing, indicating spatial and/or temporal variations in the potential. The lack of a strong correlation between the electron energy and the integrated $E_\perp$ indicates that temporal variations contribute significantly.

The first three moments of the electron distribution (density, velocity, and parallel temperature) are plotted in panels (d) to (f), respectively. These moments are derived from the energy interval from 20 to 30 keV and assume a gyrotropic plasma. The black line represent the moments derived from the measured two-dimensional (2D) distribution with no interpolation at low energies ($f=0$ for energies less than 20 eV) and the red line represents the moment calculated from the one-dimensional (1D) reduced parallel distribution with the low energy phase-space density interpolated, $f(E < 20\ \text{eV}) = f(E = 20\ \text{eV})$. A large difference between the two densities indicates the contribution of the low-energy electrons is significant.

The maximum positive slope ($df/dv_\parallel$) of the field-aligned 1D reduced electron distribution is presented in panel (g). The value of $df/dv_\parallel$ is calculated from the anti-Earthward 1D reduced electron distribution below 5 keV by using a 200 eV wide sliding window. This study has been motivated in part by these very unusual observations of persistent positive slopes. The Debye length presented in panel (h) and the field aligned current in panel (i) are both derived from the quantities in panels (d) to (f). A frequency spectrum of the electric field wave activity is plotted in panel (j).

The calculation of a positive slope in the electron distribution function depends on the ratio of the analyzer's acceptance angle with the angular extent (in pitch angle) of the electron beam. The calculations in this paper assumed the electron beams were at least as wide as the minimum angular acceptance of the EESA (6° or less). A spot check reveals that some of the electron beams were narrower, and that the values of $df/dv_\parallel$ could be lower. However, these examples were rare enough and the changes were small enough that a more tedious calculation that includes the response of the EESA would not significantly change the statistical results of this study.

B. Electron distributions

To facilitate our discussion, Fig. 3 is subdivided into three separate time periods, each characterized by different suprathermal background plasma conditions. These conditions are classified by the properties of the Earthward electrons seen in Fig. 3(b). The three time periods are delineated by the bars at the top of Fig. 3 and denoted as time period I (~20:17:46-18:02 UT), II (~20:18:08-18 UT) and III (~20:18:20-18:27 UT), respectively. The vertical black lines in Fig. 3 are intervals with missing or corrupted data which, coincidentally, are located such that they approximately separate the three periods.

Figure 4 presents four electron distributions obtained at the times indicated by the blue arrows beneath Fig. 3(c). In the left column, the 2D electron energy flux is plotted as function of energy and pitch angle. The middle and the right columns plot the perpendicular and parallel 1D, "reduced" electron distributions, obtained by assuming that the full distributions is gyrotropic then integrating the observed data in azimuthal direction (giving a 2D distribution) followed by integration over the remaining velocity dimension (i.e., parallel and perpendicular velocities, respectively). The reduced perpendicular electron distributions, while unusual, are needed to identify the warm or hot isotropic populations and to constrain the density of the field aligned populations (Sec. III C). Note that the velocity grid used here is finer than the instrument resolution.

Since the EESA also detects spacecraft-generated photoelectrons, velocities for which the field-aligned electron fluxes were below 20 eV and the perpendicular electron flux were simultaneously below 30 eV have been removed prior to computing the reduced 1D electron distributions. The 1D distributions therefore lack information about these low-energy electrons in what we will refer to as the "excluded velocity range." The dashed vertical lines in Fig. 4 mark 20 eV in energy. There are nevertheless derived fluxes identified below 20 eV (30 eV) for each energy component since only electrons with both parallel and perpendicular energy below the respective cutoffs are excluded from the analysis. The phase-space density plotted within these dashed vertical lines is lower than the actual value since a fraction of the electrons in this range have been excluded. It is therefore possible that apparent positive slope at ~20 eV are introduced in the 1D reduced distribution as a result of removing the excluded velocities. Such a positive slope would be an artifact and should not be interpreted as representing an unstable distribution. Positive slopes at other (higher) energies, however, can indicate unstable distributions, although temporal aliasing may also produce apparent positive slopes (see Sec. IV B).

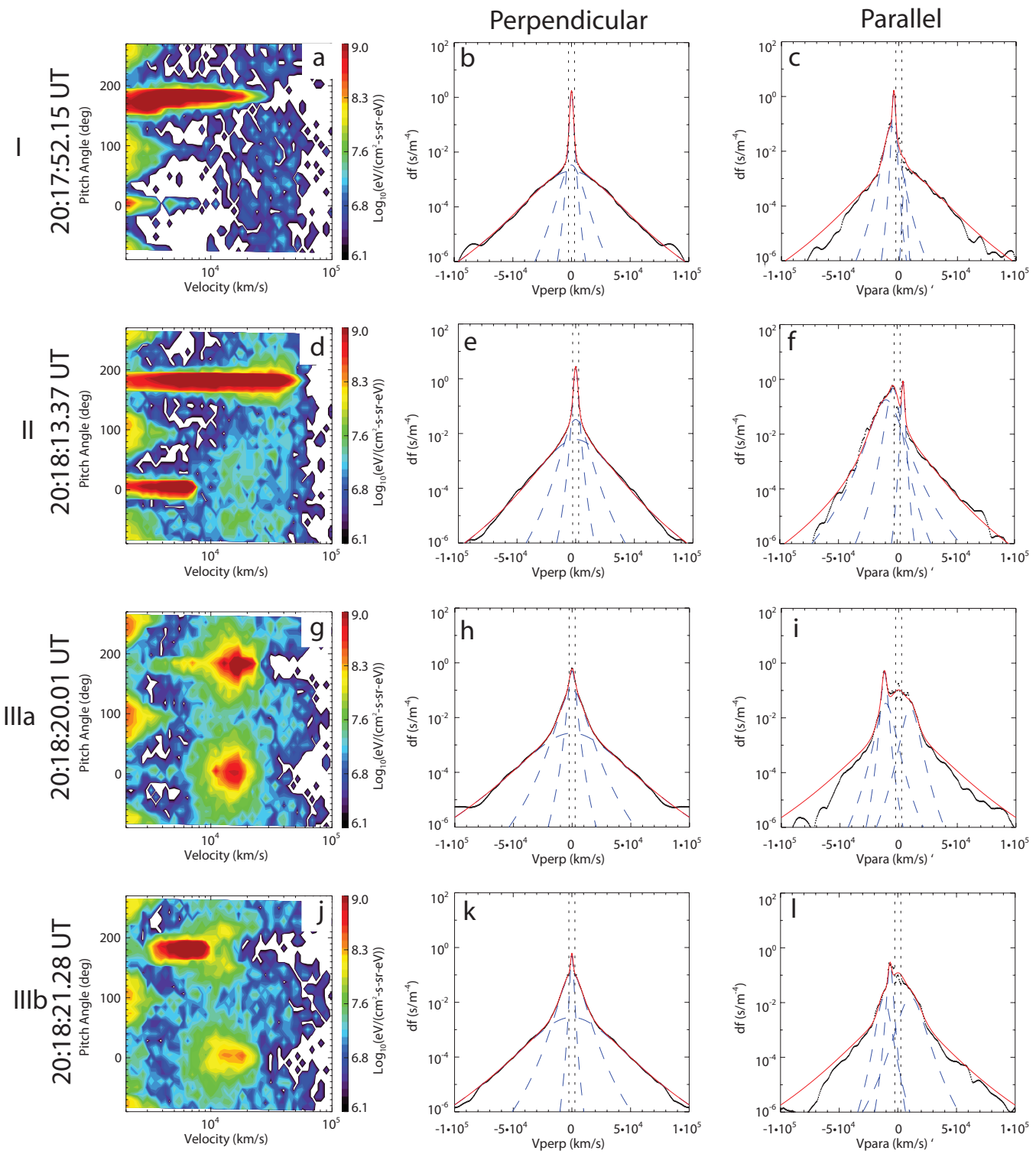

FIG. 4. (Color) Electron distributions are presented for the four times marked by the vertical blue arrows in Fig. 3. The electron distributions are shown in differing perspectives in each of the three columns. From the left to right these perspectives are as follows: (left) the 2D measured electron energy flux distribution as a function of pitch angle and velocity, (center) the 1D reduced perpendicular electron distribution function, and (right) the 1D reduced parallel electron distribution function. The blue dashed curves are fits of kappa distributions and correspond to the entries in Tables I and II, as explained in the text. The solid black curves are the functions being fit, and the solid red curves are the fits found by summing over the appropriate Kappa distributions. The dashed vertical lines indicate the 20 eV thresholds.

C. Analytical representation of the electron distributions

It is often useful to represent the electron and ion distributions in an analytical form to facilitate further investigation of plasma phenomena through use of either analytical, or numerical methods, or by means of simulations. The analytical representation employed here is designed to separate the suprathermal electron background from the field-aligned

TABLE I. The derived moments of density and temperature for the four 1D reduced perpendicular electron distributions presented in the middle column of Fig. 4. The Hot population represents plasma-sheet-like background electrons. The Warm population represents a denser background isotropic population. The Cold population represents the perpendicular velocity distribution associated with the field-aligned electron fluxes. See text for further details.

		Hot population		Warm population		Cold population	
Perp. isotropic		N (10^6 m^{-3})	T (eV)	N (10^6 m^{-3})	T (eV)	N (10^6 m^{-3})	T (eV)
1D reduced	I	0.08	2000	0.04	180	3.6	5
	II	0.3	1200	0.38	175	4	8
	IIIa	0.12	2500	1.3	210	2	20
	IIIb	0.12	2300	1.4	180	1	5

electrons. The basic idea is to fit the reduced, "perpendicular" electrons to separate a warm/hot, isotropic population from the "cold" perpendicular electrons. The density of this "cold" population which includes the field-aligned electrons, is used to restrict the densities of the field-aligned populations when the reduced, "parallel" distribution is analyzed. The observed 1D reduced electron distributions (Fig. 4), however, cannot be represented by a single analytical expression. Rather, they seem to be best represented by a sum of several Kappa (generalized Lorentzian) distributions[28] with Kappa=4. Each of the perpendicular and parallel distributions is well represented by three separate populations.

From Fig. 4 (left column), one can clearly see that there are isotropic (with one or two loss cones) and field-aligned components of the electron distributions. We isolate the isotropic part by first fitting the reduced, 1D perpendicular distributions (middle column of Fig. 4) with three nondrifting Kappa distributions: a "hot" population, a "warm" population, and a "cold" population. The hot and the warm populations are assumed to be isotropic, whereas the cold perpendicular population (which contains the field-aligned electrons) is allowed to have a more complex dependence on the parallel velocity (discussed below). The parameters of the fits are presented in Table I, with the result of each fit designed in Fig. 4 (middle column) in blue dashed lines. The sum of the three analytical distributions appears as the solid red line, which agrees well with the observed distribution (black curve) in each case.

To isolate the field-aligned population, we subtract the (assumed) isotropic hot and warm population (derived from the reduced perpendicular distributions) from the reduced 1D parallel distribution (right row of Fig. 4). The residual is fitted with three additional drifting Kappa (parallel) distributions. The total density in these three drifting Kappa distributions is constrained by the density of the previously derived cold (perpendicular) population. These parallel components are denoted the Earthward, the anti-Earthward, and the "accelerated" populations (the later also exhibiting an anti-Earthward drift). The use of the cold (perpendicular) distribution density to constrain the three drifting Kappa distributions reduces the number of degrees of freedom. In fitting the residual (field-aligned) electrons, we must separate Earthward from anti-Earthward electrons since the fluxes in the excluded velocity range are set to zero. The results of these fits are presented in Table II, with each fit drawn in Fig. 4 (right column) with blue dashed lines. The sum of the three analytical distributions plus the (assumed isotropic) hot, and the warm populations is plotted as the solid red line. The observed isotropic populations have one (or two) loss cones, as previously noted, leading to deviations at high velocities.

The isotropic hot population (Table I) can be easily identified as plasma sheet electrons [Fig. 3(b)]. In Fig. 4(a) they appear as the blue vertical band with an empty loss cone. This population exists throughout Fig. 3. The hot population has a temperature of 1–3 keV and a density of $\sim 0.01 \times 10^6$ to $\sim 0.3 \times 10^6$ m^{-3}. The relative contribution to the estimated total density (not including the measured fluxes in the excluded velocity range) is $\sim 1\%$. In the last two examples (IIIa and IIIb), the hot population has a double loss cone.

The warm population of Table I is the focus of this paper. This population has a temperature of $\sim 150-250$ eV and a density range of $\sim 0.01 \times 10^6$ to 1.4×10^6 m^{-3}. The relative abundance of this population is $\sim 1\%$ in distribution I

TABLE II. The derived moments of density, temperature, and drift velocity for the four 1D reduced parallel electron distributions in the right column of Fig. 4. Each distribution is fitted with three drifting kappa functions after the isotropic Hot and Warm population from Table I have been subtracted. The combined density of these drifting Kappa distributions is constrained by the density of the Cold perpendicular population identified in Table 1. See text for further details.

		Earthward population			Accelerated population			Anti-Earthward population		
Field-aligned (cold perp.)		N (10^6 m^{-3})	T (eV)	v_d (10^4 km/s)	N (10^6 m^{-3})	T (eV)	v_d (10^4 km/s)	N (10^6 m^{-3})	T (eV)	v_d (10^4 km/s)
1D reduced	I	0.002	5	0.5	3	4	−0.42	0.6	70	−0.64
	II	0.9	5	0.5	1.9	50	−0.5	1.2	700	−1.2
	IIIa	0.2	90	1.0	1.0	12	−1.2	0.3	100	−1.1
	IIIb	0.2	200	1.1	0.7	10	−0.66	0.1	60	−1.2

(Fig. 4), ~8% in distribution II and up to ~50% in distributions IIIa and IIIb (not including the measured fluxes in the excluded velocity range).

The shape of the anti-Earthward distributions led us to choose fits consisting of two drifting Kappa components (Table II); the anti-Earthward and the accelerated populations in Table II. These anti-Earthward electrons dominate the flow and carry the bulk of the downward current. The fit with the colder temperature of the two anti-Earthward distributions most likely represents the electron population initially accelerated by the DL. In examples I and II, the hotter of the two populations represents the thermalized or relaxed part of the initially accelerated electrons. In examples IIIa and IIIb, the hotter of the two populations represents mirrored suprathermal background electrons.

Part of the Earthward-directed electron population (Table II) may be the result of anti-Earthward electrons (accelerated by the parallel electric field) that were redirected Earthward by turbulence above the DL. These redirected electrons contribute to the trapped population in a BGK solution.[3] The Earthward population consists partly of precipitating electrons. In example I and II the precipitating electrons are seen as an isotropic population with a single loss cone; hence, they are included in the hot and warm isotropic populations (Table I). The precipitating population in examples IIIa and IIIb is mainly field aligned, leading to them predominantly being found in the Earthward population. The source of the latter precipitating electrons will be discussed in the next paragraph.

D. Earthward electrons

The source of the nonisotropic, Earthward electrons in distributions IIIa and IIIb is unknown. These electrons have higher energies then the anti-Earthward electrons so scattering by intense turbulence is unlikely. Alfvén wave acceleration was considered but there is no clear Alfvén wave signature in the observations nor any dispersion in the electron arrival time. This population could have been accelerated from the opposite hemisphere. The alternative of reflection from the opposite hemisphere, however, is unlikely since the electrons are highly field-aligned. The bounce period of a ~1 keV electron is $O(10)$ s, which can be longer than the lifetime of a DL in the downward current region. A definitive determination of the source of these electrons is beyond the scope of this paper.

IV. EFFECT OF THE HOT AND WARM ELECTRONS ON DOUBLE LAYERS

The observations in Figs. 3 and 4 allow us to investigate how a suprathermal electron population affects double layers. In region I, the density of the hot and the warm populations are negligible compared to the anti-Earthward field-aligned electrons (cold perpendicular population). In regions II and III, the hot and the warm populations are significant and positive slopes in the electron distributions sometimes persist for long periods. We scrutinize these observations to determine if and how the presence of the suprathermal electron population affects electron acceleration.

A. Self-regulated double layers

During the interval 17:46–17:52 UT (region I in Fig. 3), the characteristic electron energy is changing as the satellite moves perpendicular to $\boldsymbol{B}$. Thus, the inferred strength of the DL changes, sometimes dropping below 100 V. Part of the changing characteristic energy may be the result of spatial variations but, as explained earlier, the changes appear to be mostly temporal with a characteristic time scale of less than 1 s. The electron distributions are fully relaxed (no positive slope) in this region with very little warm suprathermal electron background.

From an analysis of a large number of anti-Earthward electron events in the downward current region with a low background of suprathermal electrons, the observed characteristic energy of the anti-Earthward electrons is often observed to change on time scales less than 1 s, frequently returning to low levels as if the accelerating potential has been disrupted. The electron energy flux spectrograms (e.g., Fig. 4, region I) indicate that the anti-Earthward particle energy flux is enhanced over a broad energy range and are fully relaxed though nonlinear evolution.

In region I, the electron population is almost entirely made up of accelerated, anti-Earthward, field-aligned electrons and the thermally relaxed population derived from them, which leads to the conclusion that the plasma environment at the DL is controlled by the DL itself. We therefore refer to this case as a self-regulated system.

The mechanism for the self-regulation of a DL appears to be a feedback loop between the ramp and the turbulent region.[1] The ramp region accelerates electrons creating an unstable distribution that will drive a nonlinear response in the turbulent region. The plasma structures and waves in the turbulent regions trap and redirect some of the accelerated electrons back to the ramp region. These redirected electrons are the "trapped" electrons in the BGK DL solution and they play a critical role in defining the potential across the DL. They also form the suprathermal electron background population for a two-stream instability in the gap-region that may generate the turbulence in the turbulent region. From this connection, one can see that the turbulent region directly affects the potential across the DL, and visa versa. Many other dynamically effects will also influence the state of the DL. Some of the effects elucidated from recent simulations[2] include the influence of fast ions on the low potential side that can drive Buneman instabilities and nonlinear interactions involving electron holes on the high-potential side that can generate ion density disruptions (with shocklike features), which in turn can destroy laminar DLs. These disruptions may play a role in the temporal evolution of the characteristic energy in the electron distribution.

B. Externally regulated double layers

In region II, the hot and warm populations contribute ~5%–10% of the total plasma density on the high-potential side of an accelerating potential, most likely a double layer. The parallel temperature moment for the 20 eV–3 keV energy range is ~200 eV, close to the temperature of the warm population of Table I. Thus, the trapped electron population

on the high-potential side that moves toward the DL is a combination of the externally supplied electrons and electrons that have been accelerated by the DL and subsequently redirected back towards the DL. We therefore regard region II as representing DL acceleration that is at least partially externally controlled.

In the region II observations, the flux from the warm population can be seen as the light blue band in Fig. 3(b) (Earthward electrons). The characteristic energy of the anti-Earthward electrons (potential across the DL) assumes a high value and remains high as long as a significant flux of suprathermal electrons are present. This is in agreement with the simulations results presented in Ref. 1. Interestingly, the characteristic energy of the accelerated electrons is roughly that of the suprathermal electron population. These observations contrast with those of Region I where the suprathermal electron population is weak and the characteristic energy varies.

The region II electron distributions [Fig. 4(d)] appear to be similar to those of region I. The accelerated electrons are distributed over a broad energy range and have little perpendicular energy. These distributions again appear to be accelerated through a potential followed by relaxation via a turbulent process.[1] There are two time periods (at ~20:1808 and 20:1812 UT) when positive slopes are identified in Fig. 3(g). This is interpreted as an artifact of a rapidly fluctuating electron distribution (i.e., temporal aliasing), due to ion cyclotron waves that are modulating the electron spectrum.[29] The ion cyclotron modulation of the electron flux, while complicating the interpretation of the observations, is unimportant relative to the influence of the suprathermal electron discussion in this paper.

Under the assumption that the electrons drifting toward the DL from the high-potential side are critical in controlling and maintaining the DL structure,[12] one can expect an externally regulated DL to behave differently than a self-regulated DL. The electron temperature and the phase-space density of the electrons flowing into the DL are not determined by the instabilities alone. Hence, one may expect the externally regulated DL to be more stable and that the suprathermal electron background exercises some control over the DL potential. Such a correlation is also suggested by the above observations and by simulations reported in a companion paper.[1] With a more well-defined temperature on the high-potential side, it is possible that the DL has a preferred potential.

C. Double layers with a strong external population

Region III (Fig. 3) is unusual in several ways. There is a dense suprathermal electron background with a high temperature [the yellow population in Fig. 3(b)] together with electron distributions that show positive slopes persisting for a long time [Fig. 3(g)]. One of the only credible explanations for these characteristics is that the satellite dwelled in the gap region (Fig. 1), just above a DL. For this to happen, the DL must have had a perpendicular extent of tens of kilometers, must have been stable for several seconds, and must have had an unusually large (along $\boldsymbol{B}$) stable gap region and/or almost no motion along $\boldsymbol{B}$ in the satellite frame, as suggested by the trajectory depicted in Fig. 1.

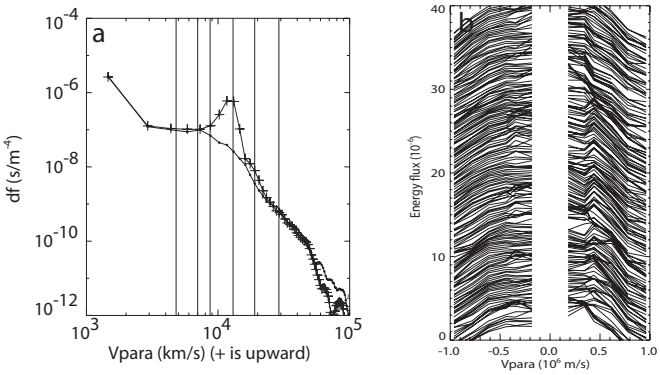

FIG. 5. Electron distributions from time period III of Fig. 3 at ~20:18:20 UT. Panel (a) contains the 1D reduced electron distribution measured by the swept energy electron instrument which makes one energy sweep every ~79 ms. The curve without crosses represents the Earthward flux and the line with crosses represents the anti-Earthward flux. The vertical lines mark the energies of the fixed-energy electron instrument, which has a time resolution of 2 ms. Panel (b) contains the field-aligned particle distribution from the fixed-energy electron instrument presented so that for each time step the distribution function is offset in the *y* direction. The negative velocity axis is Earthward and the time period covered in panel (b) is equal to 420 ms.

At the beginning of the region III period, the electron phase-space distribution has a positive slope sporadically for almost 8 s [Fig. 3(g)]. Figure 4 (IIIa and IIIb) shows examples of distributions from this interval in both 2D and 1D. Figure 4(g) (IIIa) illustrates the interaction between the DL and the Earthward-moving electrons. The externally supplied Earthward field-aligned component inside of the loss cone (seen at 0° with electron velocities below 2×10^4 km s^{-1}) is reflected by the DL. This reflected population is mixed with the accelerated electron beam from the DL (seen at 180°). The accelerated electrons at 180° and with velocities above 2×10^4 km s^{-1} have lower perpendicular temperatures and so can be distinguished from the reflected population.

In contrast, the Earthward electron population in Fig. 4(j) (IIIb) is not reflected by the DL because the energies of these electrons appears to be higher than that of the DL (inferred from the accelerated electron beam; compare 0° and 180° above 10^4 km s^{-1} in velocity). Presumably, most of these electrons are lost to the atmosphere. However, some of the suprathermal background electrons—particularly those with large enough pitch angles—mirror at lower altitude and then come back up and through the DL [Fig. 4(j), $180°\pm30°$]. These observations lend credence to our interpretation that a DL lies Earthward of the spacecraft.

The positive slopes in the electron distributions within region III are not artifacts of rapidly changing electron fluxes (i.e., sweep aliased). Instead, they are fairly stable. Another reduced, 1D, parallel distribution is displayed in Fig. 5(a). Both the measured 2D distribution and the derived 1D reduced distribution have a clear positive slope. Figure 5(b) displays the SESA (~2 ms resolution) flux measurements (six fixed energies). The six measured energies are marked by vertical lines in Fig. 5(a). Figure 5(b) covers a time period

of ~420 ms, where for each new electron distribution the curve is shifted vertically for clarity. This series of 2 ms flux measurements clearly shows that the positive slope in the electron distribution is persistent.

The positive slopes in the electron distribution function are observed continuously for 1 s and, for the following 7 s, the electron distributions have either a positive slope or a plateau distribution [Fig. 3(g)]. Such an observation is rare in the FAST data base. One would expect that the probability of making such an observation is very low since the estimated gap size from simulations is $O(10)$–$O(100)$ Debye lengths along the magnetic field. The Debye length at the time of the observations was large, i.e., ~80 m, so the gap could be on the order of 8 km along $\boldsymbol{B}$. The motion of the spacecraft along $\boldsymbol{B}$ was roughly a few kilometers, but the velocity of the DL (along $\boldsymbol{B}$) itself is expected to have been ~10 km/s, corresponding to a displacement of tens of kilometers. Therefore, we argue that, if the spacecraft stayed in the gap region (sporadically) for 1–8 s, it was due to an increased size of the gap region that cannot be only from the increase in Debye length, but also from an increased size of the gap region that is a consequence some other physical mechanism.

While unlikely, a "surfing" scenario could also be used to explain the unusually long dwell time in the gap region. Under this scenario, as the satellite travels (perpendicularly) into the next flux tube, the location of the parallel electric field location changes in such a way that the satellite (coincidentally) remains in the gap region, basically negating the fast vertical motion of DLs. Such unusual situation is illustrated in Fig. 1, where the spacecraft velocity vector, the DL's vertical motion and the DL's normal vector is directed in such way that the spacecraft can stay in the gap region for long time periods. Under any of these interpretations, the observation in Fig. 3 should be consider as unusual. Here, we choose to explore the possibility of an increased gap size.

A possible explanation for an increased gap size is that the suprathermal electron background weaken the convective instability associated with the accelerated electron beam. If the growth rate were low ($<10^3$ s^{-1}), the accelerated electrons (10^7 m s^{-1}) could travel 10–100 km before undergoing several e-folds, so the gap region could extend well beyond the typical size. Linear spatial growth rates for electron-beam-instabilities have theoretically and experimentally been shown to be affected by the suprathermal background plasma properties,[15,16] which supports our interpretation that the observed suprathermal electron background effects the gap size.

The above observations suggest that a suprathermal electron background population can affect the behavior of the accelerating potential, an interpretation that is also supported by Vlasov–Poisson DL solutions. While such an analysis is beyond the scope of this article, simulations[1] suggest that (1) a suprathermal electron background population can stabilize a DL and (2) in the presence of a strong suprathermal electron population a large gap is more likely to be formed.

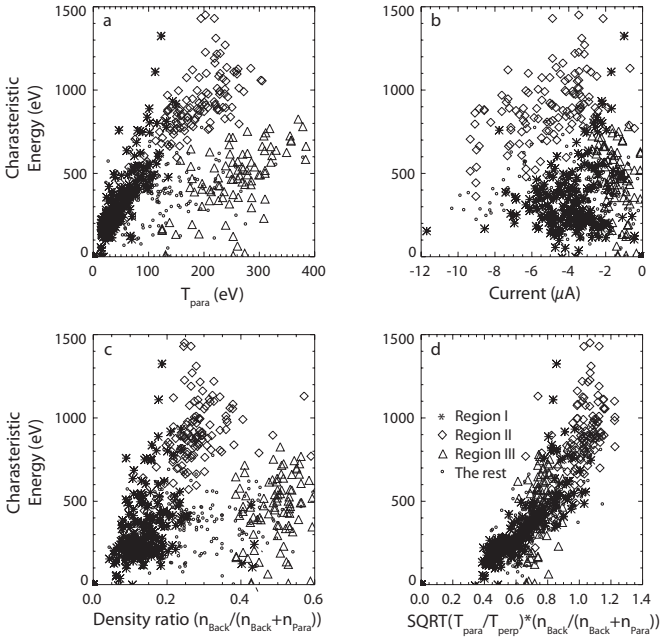

FIG. 6. Correlations between functions of the plasma distribution (e.g., moments) and the characteristic energy derived from each individual distribution of Fig. 3 are shown. The functions considered are (a) the parallel temperature, (b) the current, (c) the fraction of the density associated with the suprathermal background electrons, and (d) an empirically derived combination of the plasma moments.

V. CORRELATIONS OF DOUBLE LAYER PROPERTIES AND PLASMA CHARACTERISTICS

Figure 6 summarizes the properties of the electron distributions over the entire time period of Fig. 3. In all four plots, the y axis represents the characteristic electron energy (a proxy for the potential across the DL) and the x axis represents different plasma properties measured on the high-potential side of the DL. The symbols (star, diamond, triangle, and small circle) distinguish electron distributions from time periods I, II, III, and the distributions outside these time periods, respectively.

Here, the plasma moments are calculated from the 1D reduced distribution with the distribution function interpolated for energies <20 eV. (In contrast, the values in Tables I and II were from manual fits of kappa distributions only omitting any fluxes below 20 eV.) The phase-space density below 20 eV is set to the observed value at ±20 eV. The electron density (n_{para}), the current density ($ev_{\mathrm{para}}n_{\mathrm{para}}$), and the parallel temperature (T_{para}) are represented by the red lines in Figs. 3(d), 3(i), and 3(f) and are used in Fig. 6. Two additional values are used in Fig. 6. T_{back} and n_{back} are, respectively, the density and temperature of the isotropic suprathermal background derived from the reduced, perpendicular distributions.

Figure 6(a) compares the parallel temperature with the characteristic energy. Assuming that the characteristic energy of the electrons is indicative of the DL's potential, one can see that the T_{para} is clearly correlated to the potential in regions I and II, which share the same linear relationship. Region III is best represented by a different linear relationship. Since most of region III was from the gap region, the elec-

tron distribution was not fully relaxed. This distinction might account for at least some of the difference between regions I, II, and region III.

The current density is compared to the characteristic energy of the electrons in Fig. 6(b). No clear relationship can be seen. It is unlikely that the <20 eV electrons could account for sufficient currents to cause a correlation, so it is clear that the downward current region cannot be described with a classical Ohm's law,[30,31] particularly in regions I and III. Region II does show some correlation between current and potential.

Figure 6(c) tests for a correlation between the characteristic energy and the fraction of density in a warm/hot background. If there is a significant fraction of suprathermal background plasma on the high-potential side, the growth of the instabilities will be influenced.[15,16] For regions I and II, the probability of having a high potential across the DL increases with an increasing fraction of suprathermal background plasma. However, in region III, a different slope is seen. One interpretation of these data is that, up to a point, an increase in the fraction of suprathermal background plasma causes the potential across the DL to continue to increase. The correlation is disrupted after some threshold [~25% density level based on Fig. 6(c)] and the potential increases much more slowly. This interpretation is complicated by the fact that the temperature of the suprathermal background changes also.

The latter idea was tested by comparing the characteristic electron energy with the fraction of the suprathermal background density $n_{back}/(n_{back}+n_{para})$ modified by T_{back}. The modification $(T_{para}/T_{back})^{1/2}$ resulted a particularly good correlation [Fig. 6(d)]. This correlation indicates that the DL potential may not only be controlled by the density of the suprathermal electron background, but the degree of control [determined by the slope in Fig. 6(d)] may depend on the relative temperature of the hot and the warm electron background to the relaxed electrons. These relationships need further investigations.

VI. SUMMARY

In this paper we have interpreted electron observations in the downward current region of the aurora based on the premise that the anti-Earthward electrons are accelerated by a parallel electric field supported by a DL. We reinforced a published model of the DL by presenting four additional, previously unpublished FAST observations of localized parallel electric fields in the downward current region. These observations demonstrate the ramp region, the "gap," and the turbulent region are characteristics of DL acceleration. Based on this model, we can interpret the observation of accelerated, anti-Earthward electrons for consistency with DL acceleration in order to determine how the suprathermal electron background on the high-potential side of may affect the DL.

We have analyzed in detail a single event during which the FAST satellite was inferred to be continuously on the high-potential side of a DL in the downward current region. Based on this event, the characteristic energy of the electrons (the potential across the DL) appears to be influenced by the suprathermal background electrons.

In regions where the suprathermal electron density was negligible, the DL potential appeared to vary and return to very low levels. The electron population trapped (or reflected) by the DL potential is the result of the electrons that have been redirected back toward the DL in the turbulent region from the electron beam. These types of DL were therefore designated as self-regulated DLs. The self-regulated DL can be viewed as involving a closed connection (i.e., feedback) between the DL itself (the ramp region) and the wave activity (the turbulent region) on the high-potential side of the DL through the electrons. That is, the electron beam from the DL is responsible for the waves in the turbulent region while the redirected electrons from the beam are trapped at the DL, which effects the potential across the DL.

In regions where a significant, externally supplied suprathermal electron population is present, the DL potential appears to vary about a value characteristic of the temperature of the warm electron population. In other words, the DL appears to be externally regulated to some degree by the presence of suprathermal background electrons. Since these suprathermal background electrons comprise a significant fraction of the electron population flowing toward the DL from the high-potential side, one can envision how the DL can be more stable and less dependent on any modulations in the electron population redirected by turbulence. The DL in such cases is labeled as externally regulated. The external population may also play a role in suppressing or enhancing the instabilities such as two-stream or Buneman-like instabilities that can play a role in the disruption of the DL.

The suprathermal background electrons are supplied either by the plasma sheet or the magnetosphere electrons, depending on the latitude or longitude of the observations. The results of this study suggest that one can expect more stable potentials in the downward current region at locations where suprathermal background electrons of temperatures about 100–500 eV are present. For locations without the externally supplied suprathermal background electrons, one can expect the DL to exhibit greater temporal and/or spatial variability. Qualitative examination of additional data suggests that this phenomenon may account for why the downward current region structures at the poleward edge of the auroral oval (characterized by a low suprathermal background) are highly variable (or structured) and often very narrow in perpendicular to $\boldsymbol{B}$ extent. Larger downward current regions are more likely to be observed well inside the auroral oval where plasma sheet precipitation is common. A conclusive study needs to de undertaken to quantitatively evaluate this idea.

We also reported an unusual case of highly unstable electron distributions that endured for several seconds. The DL acceleration model offers one plausible explanation: that the spacecraft dwelled in the gap region. This observation required an unusually stable DL and an unusually large gap region, both of which are shown to occur when a strong suprathermal electron background is present in numerical simulations.[1] These results strengthen the interpretation of acceleration by DLs and of the influence of suprathermal electrons on DL stability and strength.

The observations presented in this paper are too limited to allow for a statistically conclusive interpretation. To better understand how DLs are regulated, laboratory tests and additional numerical simulations are needed. This paper shows that a suprathermal electron background population with temperatures of $O(200)$ eV is likely to play an important role in ionosphere-magnetosphere interactions but further in-depth studies by in situ missions will be required to better elucidate their role.

Finally, we note that we have not investigated whether (and if so, how) precipitating ions may also influence the DL. First, no single event has yet been found that indicates such a correlation in the same way that Fig. 3 indicates a correlation between the electrons and the DL. Second, the fact that precipitating plasma sheet electrons and ions are often co-located would complicate any statistical study intended to determine whether the changes in a DL are due to precipitating electrons or ions (or both). Without an independent observation similar to the one discussed in this paper, but for which the DL characteristics are clearly correlated with properties of the precipitating ions (but not the electrons), it is unlikely that the influence of precipitating ions on DLs can be ascertained based on observations alone. Simulations and/or laboratory experiments may therefore also be required to evaluate if ion precipitation is important for the state of the DL. Such efforts are ongoing but are outside the scope of this paper.

ACKNOWLEDGMENTS

This work has been supported by NASA Grant No. NAG5-13096 and NSF Grant No. ATM-0206906.

[1] D. L. Newman, L. Andersson, M. V. Goldman, R. E. Ergun, and N. Sen, Phys. Plasmas **15**, 072902 (2008).
[2] D. L. Newman, L. Andersson, M. V. Goldman, R. E. Ergun, and N. Sen, Phys. Plasmas **15**, 072903 (2008).
[3] I. B. Bernstein, J. M. Greene, and M. D. Kruskal, Phys. Rev. **108**, 546 (1957).
[4] M. A. Raadu, Phys. Rep. **178**, 25 (1989).
[5] R. E. Ergun, Y.-J. Su, L. Andersson, C. W. Carlson, J. P. McFadden, F. S. Mozer, D. L. Newman, M. V. Goldman, and R. J. Strangeway, Phys. Rev. Lett. **87**, 045003 (2001).
[6] L. Andersson, R. E. Ergun, D. Newman, J. P. McFadden, C. W. Carlson, and Y.-J. Su, Phys. Plasmas **9**, 3600 (2002).
[7] M. Temerin, K. Cerny, W. Lotko, and F. S. Mozer, Phys. Rev. Lett. **48**, 9585 (1982).
[8] F. S. Mozer and A. Hull, J. Geophys. Res. **106**, 5763, DOI: 10.1029/2000JA900117 (2001).
[9] R. Bostrom, G. Gustafsson, B. Holback, G. Holmgren, H. Koskinen, and P. Kintner, Phys. Rev. Lett. **61**, 82 (1988).
[10] F. S. Mozer, C. W. Carlson, M. K. Hudson, R. B. Torbert, B. Parday, J. Yatteau, and M. C. Kelley, Phys. Rev. Lett. **38**, 2599 (1977).
[11] J. P. McFadden, C. W. Carlson, R. E. Ergun, F. S. Mozer, L. Muschietti, I. Roth, and E. Mobius, J. Geophys. Res. **108**, 8018, DOI: 10.1029/2002JA009485 (2003), 2003.
[12] D. L. Newman, M. V. Goldman, R. E. Ergun, and A. Mangeney, Phys. Rev. Lett. **87**, 255001 (2001).
[13] R. E. Ergun, L. Andersson, D. Main, Y.-J. Su, D. L. Newman, M. V. Goldman, C. W. Carlson, J. P. McFadden, and F. S. Mozer, Phys. Plasmas **9**, 3685 (2002).
[14] A. J. Hull, J. W. Bonnell, F. S. Mozer, and J. D. Scudder, J. Geophys. Res. **108**, 1007, DOI: 10.1029/2001JA007540 (2003).
[15] T. M. O'Neil and J. H. Malmberg, Phys. Fluids **11**, 1754 (1968).
[16] P. Y. Cheung and A. Y. Wong, Phys. Fluids **28**, 1538 (1985).
[17] N. Singh and H. Thiemann, Geophys. Res. Lett. **7**, 737, DOI: 10.1029/GL007i010p00737 (1980).
[18] R. E. Ergun, C. W. Carlson, J. P. McFadden F. S. Mozer *et al.*, Geophys. Res. Lett. **25**, 2041, DOI: 10.1029/98GL00636 (1998).
[19] G. Marklund, L. Blomberg, C.-G. Fälthammar, and P.-A. Lindqvist, Geophys. Res. Lett. **21**, 1859, DOI: 10.1029/94GL00194 (1994).
[20] C. W. Carlson, J. P. McFadden, R. E. Ergun *et al.*, Geophys. Res. Lett. **25**, 2017, DOI: 10.1029/98GL00851 (1998).
[21] L. Andersson and R. E. Ergun, J. Geophys. Res. **111**, A07203, DOI: 10.1029/2005JA011261 (2006).
[22] C. W. Carlson, R. F. Pfaff, and J. G. Watzin, Geophys. Res. Lett. **25**, 2013, DOI: 10.1029/98GL01592 (1998).
[23] C. W. Carlson, J. P. McFadden, D. Everett, D. W. Curtis, and A. Magoncelli, Space Sci. Rev. **98**, 33 (2001).
[24] R. E. Ergun, C. W. Carlson, F. S. Mozer *et al.*, Space Sci. Rev. **98**, 67 (2001).
[25] R. C. Elphic, J. D. Means, R. C. Snare, R. J. Strangeway, and L. Kepko, Space Sci. Rev. **98**, 151 (2001).
[26] R. E. Ergun, L. Andersson, C. W. Carlson, D. L. Newman, and M. V. Goldman, Curr. Mod. Biol. **10**, 45 (2003).
[27] C. W. Carlson, J. P. McFadden, R. E. Ergun, M. Temerin, W. Peria, F. S. Mozer, D. M. Klumpar, E. G. Shelly, W. K. Peterson, E. Moebius, R. Elphic, R. Strangway, C. Cattell, and R. Pfaff, Geophys. Res. Lett. **25**, 2017, DOI: 10.1029/98GL00851 (1998).
[28] D. Summers and R. M. Thorne, Phys. Fluids B **3**, 1835 (1991).
[29] J. P. McFadden, C. W. Carlson, and R. E. Ergun, J. Geophys. Res. **104**, 14453, DOI: 10.1029/1998JA900167 (1999).
[30] R. C. Elphic, J. W. Bonnell, R. J. Strangeway *et al.*, Geophys. Res. Lett. **25**, 2033, DOI: 10.1029/98GL01158 (1998).
[31] M. Temerin and C. W. Carlson, Geophys. Res. Lett. **25**, 2365, DOI: 10.1029/98GL01865 (1998).